Research Square

Preprints are preliminary reports that have not undergone peer review.
They should not be considered conclusive, used to inform clinical practice,
or referenced by the media as validated information.

Impact of Manganese Incorporation on Structural, Optical and Magnetic Features of ZnO Nanoparticles

Nishad K K
MES College
Sapna P
MG College
Rashida T N K
Sree Narayana College
Muhammed Arif P
MES College
Midhun H
MES College
Joshy Joseph
joshyj@nirmalagiricollege.ac.in

Nirmalagiri College

Research Article

Keywords: ZnO nanoparticles, Ferromagnetism, Mn doping, Optical properties, Dilute Magnetic Semiconductors

Posted Date: August 25th, 2026

DOI: https://doi.org/10.21203/rs.3.rs-10578907/v1

License: This work is licensed under a Creative Commons Attribution 4.0 International License.
Read Full License

Additional Declarations: No competing interests reported.

Abstract

ZnO nanoparticles doped with Mn at different concentrations were successfully synthesizedvia solution based approach. The structural, optical and magnetic properties were systematically investigated using X-ray diffraction (XRD), UV-visible absorption spectroscopy, photoluminescence spectroscopy and vibrating sample magnetometry (VSM). XRD analysis confirmed a pure wurtzite crystal structure without any impurity phases and the average particle size ranged from 5.8 to 6 nm. Optical absorption studies revealed a red shift in the absorption edge with increasing Mn concentration, attributed to strong exchange interactions between Mn d-electrons and the host band electrons. Photoluminescence spectra showed characteristic band edge emission and defect-related green emission, with the latter being quenched upon Mn doping. All samples exhibited room temperature ferromagnetism, with saturation magnetization increasing from 0.032 emu/cm³ for undoped ZnO to 0.95 emu/cm³ for 3% Mn-doped samples. The observed ferromagnetism is discussed in terms of bound magnetic polarons mediated by shallow donor electrons.

1. Introduction

Dilute magnetic semiconductors (DMS) have emerged as a promising class of materials, combining the functionality of semiconductors with mild magnetic properties, making them ideal for spintronic technology development [1]. These DMS materials offer a unique blend of benefits: magnetism enables data storage, while their semiconducting nature facilitates rapid processing and sensor applications [2]. Among DMS materials, ZnO-based systems have shown exceptional potential in spintronics due to their non-volatility, faster operation, low power consumption and high integration density [3]. ZnO, a luminescent semiconductor with a wide band gap at room temperature and high exciton binding energy, stands out for its distinctive piezoelectric, electrical and optical attributes [4]. Its nanomaterials have multifunctional applications, making it an attractive host material for DMS. The incorporation of transition metals like manganese (Mn) can further enhance ZnO's magnetic and optical properties, making it suitable for advanced spintronic devices [5].

Fabricating ZnO nanostructures in reduced dimensions, especially nanoparticles incorporating 3d transition metal dopants, carries substantial value for advancing spintronic applications at the nanoscale [6]. The doping of transition metal into wide band gap oxides has been shown to propagate carrier-induced ferromagnetism [7–9]. Luo et al. produced Mn-doped ZnO (ZnMnO) nanoparticles averaging around 40 nm in size via a combustion synthesis technique; however, magnetic analysis revealed antiferromagnetic behavior in these particles [10]. Coey et al. suggested a donor impurity band exchange mechanism in oxide DMS, wherein shallow donor electrons mediate ferromagnetic coupling by forming overlapping bound magnetic polarons that generate a spin-split impurity band [11, 12]. The efficiency of Mn doping in ZnO nanocrystals depends on several factors, including the surfactant in the growth solution and nanocrystal shape [13, 14]. The maximum magnetic moment is observed when the Mn concentration is less than 3 weight% in the ZnO sample matrix [15].

Few studies have explored the magnetic characteristics of organic-capped oxide nanocrystals, leaving the true source of ferromagnetism poorly understood [16–19]. Although recent literature frequently describes transition metal-doped ZnO DMS thin films, high-quality nanoscale powders displaying room-temperature ferromagnetism (RT-FM) remain scarce [20–22].

This research details the preparation and magnetic behavior of Mn-doped ZnO nanoparticles synthesized via simple solution-phase route [23]. Various dopant levels were examined through X-ray diffraction (XRD), vibrating sample magnetometry (VSM), UV-visible absorption and photoluminescence analyses to characterize their structural, magnetic and optical traits.

2. Materials and methods

For ZnO nanoparticle synthesis, the precursors consisted of 0.05 M zinc acetate (ZnAc, analytical reagent grade) and 0.1 M sodium hydroxide dissolved in anhydrous ethanol. Particle dimensions were tuned by adding a specific quantity of dodecylamine (DDA) in absolute ethanol as part of the preparation process [24]. The concentrations of ZnAc:DDA was kept at molar ratio 1:1 and the sample name denoted as M0. For Mn doping, manganese acetate supplemented to provide Mn^{2+} ions in ZnO nanoparticles [25]. A series of samples were prepared with controlled Mn content (in molar %) of 0.5, 1.0, 2.0 and 3% and the sample were designated as M1, M2, M3 and M4. The excess zinc acetate and sodium ions were removed through multiple washes with ethanol and acetone.

3. Results and discussion

3.1 Structural properties

The XRD patterns for undoped ZnO nanoparticles (M0) and Zn1-xMnxO nanoparticles (M1, M2, M3 and M4) are shown in Fig. 1. The diffraction peaks for the undoped sample match well with the wurtzite structure of ZnO (space group P63mc, JCPDS File No. 186) [26, 27]. The Miller plane assignments for the peaks have also been shown in the Fig. 1. No peaks corresponds to any extra phase was observed in any sample, which indicates that phase-pure doped nanocrystals were obtained by this synthetic scheme [28, 29].

XRD shows a systematic XRD peak shift towards lower angle side is observed with increasing the dopant concentration indicates increases in the average inter planar distance in the corresponding planes [28]. No changes in the broadening in the XRD peaks with the increase in the dopant concentration, which may due to decrease in the particle size. The average crystallite sizes, calculated using Scherrer's formula from the three strongest peaks, were found to be 5.8 nm, 5.8 nm, 6.0 nm, 6.0 nm for samples M0, M1, M2, M3 and M4, respectively, consistent with previous reports [30].

The shift in XRD peaks towards lower angles with increasing Mn concentration suggests that Mn ions are successfully substituting Zn ions in the ZnO lattice, leading to lattice expansion. This expansion can

be attributed to the larger ionic radius of Mn^{2+} (0.80 Å) compared to Zn^{2+} (0.74 Å) [31]. The absence of any impurity peaks and the systematic peak shift indicate that the Mn doping does not introduce any significant lattice distortion or phase separation, resulting in high-quality doped nanocrystals [32]. These results are crucial for understanding the structural properties of Mn-doped ZnO nanoparticles and their potential applications in spintronic devices [33].

Table 1
XRD indexed results from sample M0, M1, M3 and M4

Sample	2θ	d value (A^0)		Miller palne	Component	Phase	Crystallite size(nm)
		Obsd	Std				
M0	31.73	2.81	2.81	(100)	ZnO	Wurtzite	5.8
	34.57	2.59	2.60	(002)			
	36.16	2.48	2.47	(101)			
	47.55	191	1.91	(102)			
	56.5	1.62	1.62	(110)			
	62.72	1.48	1.47	(103)			
	67.8	1.38	1.37	(112)			
M1	31.05	2.87		(100)	ZnO	Wurtzite	5.8
	33.81	2.65		(002)			
	35.5	2.52		(101)			
	46.8	1.93		(102)			
	55.8	1.64		(110)			
	62.22	1.49		(103)			
	67.41	1.38		(112)			
M3	30.46	2.93		(100)	ZnO	Wurtzite	5.9
	33.16	2.69		(002)			
	34.87	2.57		(101)			
	46.25	1.96		(102)			
	55.22	1.66		(110)			
	61.54	1.50		(103)			
	66.92	1.40		(112)			
M4	30.35	2.94		(100)	ZnO	Wurtzite	5.9
	33.16	2.70		(002)			
	34.87	2.57		(101)			
	46.28	1.96		(102)			
	55.29	1.66		(110)			

61.54	1.54	(103)
66.8	1.34	(112)

3.2 Optical properties

The optical absorption spectra of Mn-doped ZnO nanocrystals at room temperature are shown in Fig. 2. All spectra exhibit a sharp absorption onset in the ultraviolet region, accompanied by well-defined exciton peaks. The absorption onset of undoped ZnO nanoparticles was observed at 366 nm, which progressively blue-shifted with increasing Mn concentration in the ZnO matrix. This blue shift can be attributed to the modification of the electronic structure of ZnO due to Mn doping [32]. The absorption onsets for samples M0, M1, M2, M3 and M4 were observed at 366 nm, 356 nm, 350 nm, 345 nm and 339 nm, respectively, corresponding to band gap energies of 3.39 eV, 3.48 eV, 3.54 eV, 3.59 eV and 3.66 eV. The increase in band gap energy with increasing Mn concentration suggests a modification of the electronic structure of ZnO due to Mn doping [34]. The observed blueshift in the absorption onset with increasing Mn concentration, corresponding to an increase in band gap energy, suggests that Mn doping is modifying the electronic structure of ZnO. This increase in band gap energy can be attributed to several factors. One possible explanation is the Burstein-Moss effect, where the Fermi level shifts into the conduction band as the doping concentration increases, leading to an increase in the band gap energy [35]. Another factor to consider is the strong exchange interactions between the d electrons of Mn and the s and p electrons of the host band [36]. These interactions can lead to a modification of the band structure, resulting in an increase in band gap energy. The fact that the particle size is not significantly changing, as indicated by XRD results, suggests that quantum confinement effects may not be the primary reason for the observed blue shift [37]. The contrast between these results and previous reports on Mn-doped ZnO nanorods, where different observations were made, highlights the complexity of doping-induced modifications in nanocrystals. The differences could be due to variations in synthesis methods, particle size, shape, or doping concentrations [38].

The electronic transitions in undoped and Mn-doped ZnO nanoparticles were investigated using photoluminescence (PL) spectroscopy, with results shown in Fig. 3. The emission spectra of undoped ZnO nanoparticles exhibited two bands: a weak UV emission peak (E1) and a strong green emission peak (E2). The UV emission peak (E1) arises from band-edge emission, as its position aligns closely with the absorption onset. The green emission peak (E2) likely originates from localized deep trap states, such as singly ionized oxygen vacancies [39].

Table 2 summarizes the experimentally determined emission peak positions and corresponding absorption onsets for samples M0–M4. Earlier studies have explored the blue-green emission and associated trap states in ZnO [40, 41]. The widely accepted mechanism for green emission involves electron transitions from the conduction band minimum to the valence band maximum, mediated oxygen vacancies [42].

It is instructive to compare the normalized peak intensity ratios E_2/E_1 for samples M0 to M4. The results have been shown in Fig. 4. Upon the inclusion of Mn2 + ions, the green emission band of ZnO nanoparticles diminished. The disappearance of green emission band in Mn-doped ZnO nanorods is because Mn is a strong quencher of the luminescence of ZnO. It is also noticed that a new peak centered at 670 nm appeared for higher doped samples M3 and M4. This red emission in Mn-doped ZnO nanoparticles can be assigned tothe $^4T_1$ -$^6A_1$ transition in Mn^{2+} ions [43].

The observed absorption edges, UV emission peaks (E1) and trap emission peaks (E2) for all samples are summarized in Table 2. These data reveal a consistent blueshift in both the absorption onset and UV emission peak (E1) with increasing Mn concentration, while the green emission peak (E2) position remains relatively stable [44]. These findings highlight how Mn doping tunes the optical properties of ZnO nanoparticles.

Table 2
The observed absorption edge, UV emission peak (E_1) and trap emission peak (E_2) for ZnO nano particles samples M0 to M4.

Sample	Absorption onset	PL peak position	
		E1	E2
M0	343	350	529
M1	347	351	523
M2	349	358	532
M3	353	359	537
M4	356	359	--

3.2 Magnetic properties

Magnetic properties of the as-prepared ZnO nanoparticles were characterized using a superconducting quantum interference device (SQUID-VSM) magnetometer in thin-film attachment mode. Figure 5 displays the magnetization versus applied magnetic field for the undoped ZnO sample (M0) and Mn-doped samples (M1–M4) measured at 300 K. After subtracting the diamagnetic background, all samples (M0–M4) showed clear ferromagnetic behavior, as indicated by the presence of hysteresis loops [45]. The coercive field (Hc), remanent magnetization (Mr) and saturation magnetization (Ms) values extracted from these hysteresis loops are listed in Table 3. These parameters increase progressively with rising Mn dopant concentration, signaling enhanced ferromagnetic ordering in samples with higher doping levels [46]. For instance, the saturation magnetization (Ms) of the undoped sample (M0) measures 1.18 emu/cm³, rising notably in the doped samples.

Figure 6 illustrates the size dependence of the hysteresis loop area for the undoped sample and doped samples M1–M4. As anticipated, the loop area expands substantially with doping, further confirming

strengthened magnetism [47].

Table 3
Saturation magnetization (Ms), Remnant magnetization (Mr) and Coercivity (Hc) for samples

Sample name	Ms (emu/cm^3)	Mr (emu/cm^3)	Hc (Oe)
M0	0.03	0.001	20.9
M1	0.37	0.003	5.0
M2	0.52	0.012	12.4
M3	0.68	0.039	21.8
M4	0.95	0.041	25.2

Notably, the undoped sample displays a measurable hysteresis loop area that expands dramatically in heavily Mn-doped samples. The origin of room-temperature ferromagnetism in undoped ZnO nanoparticles remains unclear. In undoped ZnO nanocrystals, possible ferromagnetic ordering has been linked to positional defects or direct interactions among bound magnetic polarons (BMPs) [48].

In wide-band-gap materials like ZnO nanoparticles, long-range ferromagnetic ordering may arise from indirect BMP interactions mediated by magnetic impurities. However, this requires a high density of spin-polarized impurities within the host lattice. The observed results align with a novel form of defect-induced ferromagnetism driven by abundant oxygen vacancies [49]. This ferromagnetism is facilitated by shallow donor electrons that form overlapping BMPs, creating a spin impurity band. While Mn doping alone typically produces n-type ZnO, intrinsic defects such as oxygen vacancies and Zn interstitials also serve as shallow donors. In ZnMnO nanoparticles, room-temperature ferromagnetism emerges from long-range ferromagnetic coupling between Mn2 + ions, mediated by these shallow donor electrons [50].

4. Conclusion

Mn-doped ZnO nanoparticles with varying dopant concentrations (0–3 mol%) were successfully synthesized using a simple solution phase method. Structural analysis confirmed phase-pure wurtzite ZnO with systematic lattice expansion upon Mn incorporation. The average particle size ranged from 5.8 to 6.0 nm. Optical absorption studies revealed red shifts in the absorption edge with increasing Mn concentration, attributed to sp-d exchange interactions. Photoluminescence measurements showed characteristic band edge and defect-related emissions, with Mn^{2+} ions acting as efficient quenchers of green emission.

All samples exhibited room temperature ferromagnetism, with saturation magnetization increasing systematically from 0.032 emu/cm³ for undoped ZnO to 0.945 emu/cm³ for 3% Mn-doped samples. The observed ferromagnetism is attributed to bound magnetic polarons mediated by shallow donor electrons from oxygen vacancies. These results demonstrate that Mn-doped ZnO nanoparticles are promising candidates for spintronic applications.

Declarations

Conflict of interest

On behalf of all authors, the corresponding author states that there is no conflict of interest.

Data access statement

All data generated during this study are included in the manuscript.

Ethics, Consent to Participate, and Consent to Publish declarations: not applicable

Author Contribution

Joshy Joseph contributed to conceptualization and methodology adopted in the present study.Nishad K K performed the study in detail and made data collectionSapna P added some meaningful contribution in the XRD analysisRashida T N K elaborated magnetic study in detailMuhammed Arif P and Midhun H performed formal analysis and writing of the original draft.All authors reviewed, edited, and approved the final manuscript.

References

1. Gupta A, Zhang R, Kumar P, Kumar V, Kumar A. Nano-Structured dilute magnetic semiconductors for efficient spintronics at room temperature. Magnetochemistry. 2020;6(1):15. https://doi.org/10.3390/magnetochemistry6010015.
2. Jia Z, Zhao M, Chen Q, Tian Y, Liu L, Zhang F, Zhang D, Ji Y, Camargo B, Ye K, Sun R, Wang Z, Jiang Y. Spintronic Devices upon 2D Magnetic Materials and Heterojunctions. ACS Nano. 2025;19(10):9452–83. https://doi.org/10.1021/acsnano.4c14168.
3. Wahba MA, Yakout S, Sheta SM, Helal A, El-Sheikh SM. Robust ferromagnetic V0.05-XCoxZn0.95O (x = 0.01, 0.02, 0.03, 0.04, 0.05) nano-compounds: New dilute magnetic-semiconductors with tailored optical activity. J Alloys Compd. 2024;1003:175503. https://doi.org/10.1016/j.jallcom.2024.175503.
4. Goel S, Kumar B. A review on piezo-/ferro-electric properties of morphologically diverse ZnO nanostructures. J Alloys Compd. 2019;816:152491. https://doi.org/10.1016/j.jallcom.2019.152491.
5. Gallegos MV, Luna CR, Peluso MA, Damonte LC, Sambeth JE, Jasen PV. Effect of Mn in ZnO using DFT calculations: Magnetic and electronic changes. J Alloys Compd. 2019;795:254–60. https://doi.org/10.1016/j.jallcom.2019.05.044.
6. Muktaridha O, Adlim M, Suhendrayatna S, Ismail I. Progress of 3d metal-doped zinc oxide nanoparticles and the photocatalytic properties. Arab J Chem. 2021;14(6):103175.

https://doi.org/10.1016/j.arabjc.2021.103175.

7. Singh S, Deepthi JD, Ramachandran B, Rao R. Synthesis and comparative study of Ho and Y doped ZnO nanoparticles. Mater Lett. 2011;65(19–20):2930–3. https://doi.org/10.1016/j.matlet.2011.06.006.
8. Pearton S, Abernathy C, Thaler G, Frazier R, Ren F, Hebard A, Park Y, Norton D, Tang W, Stavola M, Zavada J, Wilson R. Effects of defects and doping on wide band gap ferromagnetic semiconductors. Phys B Condens Matter. 2003;340–2. https://doi.org/10.1016/j.physb.2003.09.003.
9. Ogale SB. Dilute doping, defects, and ferromagnetism in metal oxide systems. Adv Mater. 2010;22(29):3125–55. https://doi.org/10.1002/adma.200903891.
10. Luo X, Lee W, Xing G, Bao N, Yonis A, Chu D, Lee J, Ding J, Li S, Yi J. Ferromagnetic ordering in Mn-doped ZnO nanoparticles. Nanoscale Res Lett. 2014;9(1):625. https://doi.org/10.1186/1556-276x-9-625.
11. Coey JMD, Wongsaprom K, Alaria J, Venkatesan M. Charge-transfer ferromagnetism in oxide nanoparticles. J Phys D Appl Phys. 2008;41(13):134012. https://doi.org/10.1088/0022-3727/41/13/134012.
12. Coey JMD, Venkatesan M, Fitzgerald CB. Donor impurity band exchange in dilute ferromagnetic oxides. Nat Mater. 2005;4(2):173–9. https://doi.org/10.1038/nmat1310.
13. Popescu T, Matei CO, Vlaicu ID, Tivig I, Kuncser AC, Stefan M, Ghica D, Miclea LC, Savopol T, Culita DC, Moisescu MG. Influence of surfactant-tailored Mn-doped ZnO nanoparticles on ROS production and DNA damage induced in murine fibroblast cells. Sci Rep. 2020;10(1):18062. https://doi.org/10.1038/s41598-020-74816-0.
14. Carofiglio M, Barui S, Cauda V, Laurenti M. Doped Zinc oxide nanoparticles: synthesis, characterization and potential use in nanomedicine. Appl Sci. 2020;10(15):5194. https://doi.org/10.3390/app10155194.
15. Sharrouf M, Awad R, Marhaba S, Bakeer DE. Structural, optical and room temperature magnetic study of MN-Doped ZNO nanoparticles. NANO. 2015;11(04):1650042. https://doi.org/10.1142/s1793292016500429.
16. Stiufiuc GF, Stiufiuc RI. Magnetic nanoparticles: synthesis, characterization, and their use in biomedical field. Appl Sci. 2024;14(4):1623. https://doi.org/10.3390/app14041623.
17. Vasić K, Knez Ž, Leitgeb M. Multifunctional iron oxide nanoparticles as promising magnetic biomaterials in drug delivery: a review. J Funct Biomaterials. 2024;15(8):227. https://doi.org/10.3390/jfb15080227.
18. K NK, Manthrammel MA, Shkir M, AlFaify S, Pandey R. Effect of organic capping on defect induced ferromagnetism in ZnO nanoparticles. Phys B Cond Mat. 2021;624:413379. https://doi.org/10.1016/j.physb.2021.413379.
19. Hosny AA, El-Deeb B, Mohamed ZA, Hassan A, Kamel M, Elbeltagi S, Saadallah HaA, Ibrahim E. Green synthesis of Mn-doped iron oxide nanoparticles using sugarcane juice for magnetic

hyperthermia applications. Sci Rep. 2025;15(1):28686. https://doi.org/10.1038/s41598-025-11998-5.

20. De Godoy M, Gratens X, Chitta V, Mesquita A, De Lima M, Cantarero A, Rahman G, Morbec J, De Carvalho H. Defect induced room temperature ferromagnetism in high quality Co-doped ZnO bulk samples. J Alloys Compd. 2020b;859:157772. https://doi.org/10.1016/j.jallcom.2020.157772.
21. Pearton S, Norton D, Ivill M, Hebard A, Zavada J, Chen W, Buyanova I. Ferromagnetism in Transition-Metal Doped ZNO. J Electron Mater. 2006;36(4):462–71. https://doi.org/10.1007/s11664-006-0034-z.
22. Abdel-Baset TA, Fang Y, Anis B, Duan C, Abdel-Hafiez M. Structural and Magnetic Properties of Transition-Metal-Doped Zn 1 – x Fe x O. Nanoscale Res Lett. 2016;11(1):115. https://doi.org/10.1186/s11671-016-1332-x.
23. Moontragoon P, Pinitsoontorn S, Thongbai P. Mn-doped ZnO nanoparticles: Preparation, characterization, and calculation of electronic and magnetic properties. Microelectron Eng. 2013;108:158–62. https://doi.org/10.1016/j.mee.2013.01.061.
24. Mahamuni PP, Patil PM, Dhanavade MJ, Badiger MV, Shadija PG, Lokhande AC, Bohara RA. Synthesis and characterization of zinc oxide nanoparticles by using polyol chemistry for their antimicrobial and antibiofilm activity. Biochem Biophys Rep. 2018;17:71–80. https://doi.org/10.1016/j.bbrep.2018.11.007.
25. Menon M, John DM, Sreekanth K, Sivasubramanian G, Sajna P, Dharan SS, Sathyan S, Devika L, Aiswarya S, Raja K, Sreedhar K. (2022). ZnO and Mn doped ZnO generated under three different synthesis conditions and photocatalytic reduction of hazardous hexavalent chromium by these photocatalysts. *Materials Today Proceedings*, *66*, 2374–2380. https://doi.org/10.1016/j.matpr.2022.06.333
26. P GK, Thamizselvi SM, R., Sen DB. Antimicrobial studies and characterization of ZnO nanoparticles by chemical method. GSC Adv Res Reviews. 2021;8(2):071–7. https://doi.org/10.30574/gscarr.2021.8.2.0150.
27. Luo X, Lee W, Xing G, Bao N, Yonis A, Chu D, Lee J, Ding J, Li S, Yi J. Ferromagnetic ordering in Mn-doped ZnO nanoparticles. Nanoscale Res Lett. 2014;9(1):625. https://doi.org/10.1186/1556-276x-9-625.
28. Jung MK, Park Y, Lee CE, Song DS, Park S, Park C, Kim JH, Myung S, Park J, Kim CG, Lim J. Growth of phase-pure β-NiS thin films via single-source MOCVD and enhanced substrate interaction for electrocatalytic hydrogen evolution. Appl Surf Sci. 2025b;709:163873. https://doi.org/10.1016/j.apsusc.2025.163873.
29. Bhukkal C, Ahlawat R. Cu2+–Mn2+-Co-doped CdO nanocrystallites: comprehensive research on phase, morphology and optoelectronic properties. Res Chem Intermed. 2020;46(9):4211–32. https://doi.org/10.1007/s11164-020-04202-y.
30. Alam MA, Ahmed S, Bishwas RK, Mostofa S, Jahan SA. X-ray crystallographic diffraction study by whole powder pattern fitting (WPPF) method: Refinement of crystalline nanostructure polymorphs

TiO2. S Afr J Chem Eng. 2024;51:68–77. https://doi.org/10.1016/j.sajce.2024.10.010.

31. Gallegos MV, Peluso MA, Thomas H, Damonte LC, Sambeth JE. Structural and optical properties of ZnO and manganese-doped ZnO. J Alloys Compd. 2016;689:416–24. https://doi.org/10.1016/j.jallcom.2016.07.283.
32. Aadnan I, Zegaoui O, Mragui AE, Daou I, Moussout H, Da Silva JCGE. Structural, Optical and Photocatalytic Properties of Mn Doped ZnO Nanoparticles Used as Photocatalysts for Azo-Dye Degradation under Visible Light. Catalysts. 2022;12(11):1382. https://doi.org/10.3390/catal12111382.
33. Ahmed S. Structural, optical, and magnetic properties of Mn-doped ZnO samples. Results Phys. 2017;7:604–10. https://doi.org/10.1016/j.rinp.2017.01.018.
34. Akram R, Fatima A, Almohaimeed ZM, Farooq Z, Qadir KW, Zafar Q. (2023). Photocatalytic Degradation of Methyl Green Dye Mediated by Pure and Mn-Doped Zinc Oxide Nanoparticles under Solar Light Irradiation. Adsorption Science & Technology, 2023. https://doi.org/10.1155/2023/5069872
35. Zhai C, Zhang R, Chen X, Zheng Y, Wang S, Liu J, Dai N, Chen L. Effects of AL doping on the properties of ZNO thin films deposited by atomic layer deposition. Nanoscale Res Lett. 2016;11(1):407. https://doi.org/10.1186/s11671-016-1625-0.
36. Sabri NS, Yahya AK, Talari MK. Emission properties of Mn doped ZnO nanoparticles prepared by mechanochemical processing. J Lumin. 2012;132(7):1735–9. https://doi.org/10.1016/j.jlumin.2012.02.020.
37. Abdullah BJ. Size effect of band gap in semiconductor nanocrystals and nanostructures from density functional theory within HSE06. Mater Sci Semiconduct Process. 2021;137:106214. https://doi.org/10.1016/j.mssp.2021.106214.
38. Alali HA, Tiss F, Omri K, Alamer K, Alhashem ZH. Effect of Mn doping on microstructure and photocatalytic properties of ZnO nanoparticles synthesized via a hydrothermal method. Mater Res Express. 2024;11(12):125005. https://doi.org/10.1088/2053-1591/ad9fd8.
39. Raji R, Gopchandran K. ZnO nanostructures with tunable visible luminescence: Effects of kinetics of chemical reduction and annealing. J Sci Adv Mater Devices. 2017;2(1):51–8. https://doi.org/10.1016/j.jsamd.2017.02.002.
40. Rakshit S, Vasudevan S. Trap-State Dynamics in Visible-Light-Emitting ZNO:MGO Nanocrystals. J Phys Chem C. 2008;112(12):4531–7. https://doi.org/10.1021/jp7109109.
41. Chen H, Ding J, Guo W, Chen G, Ma S. Blue-green emission mechanism and spectral shift of Al-doped ZnO films related to defect levels. RSC Adv. 2013;3(30):12327. https://doi.org/10.1039/c3ra40750k.
42. Pramanik S, Mondal S, Mandal AC, Mukherjee S, Das S, Ghosh T, Nath R, Ghosh M, Kuiri PK. Role of oxygen vacancies on the green photoluminescence of microwave-assisted grown ZnO nanorods. J Alloys Compd. 2020;849:156684. https://doi.org/10.1016/j.jallcom.2020.156684.

43. Acharya SA, Dani A, Sayyed SK, Gaikawad VM. (2013). Understanding the role of mode of heating on phase formation of FE–PT nanoparticles. In *Springer proceedings in physics* (pp. 51–63). https://doi.org/10.1007/978-3-642-34216-5_5
44. Farooqi MMH, Srivastava RK. Enhanced UV–vis photoconductivity and photoluminescence by doping of samarium in ZnO nanostructures synthesized by solid state reaction method. Optik. 2016;127(8):3991–8. https://doi.org/10.1016/j.ijleo.2016.01.074.
45. Wang B, Xia C, Iqbal J, Tang N, Sun Z, Lv Y, Wu L. Influences of Co doping on the structural, optical and magnetic properties of ZnO nanorods synthesized by hydrothermal route. Solid State Sci. 2009;11(8):1419–22. https://doi.org/10.1016/j.solidstatesciences.2009.04.024.
46. Buzinaro M, Ferreira N, Cunha F, Macêdo M. Hopkinson effect, structural and magnetic properties of M-type Sm3+-doped SrFe12O19 nanoparticles produced by a proteic sol–gel process. Ceram Int. 2015;42(5):5865–72. https://doi.org/10.1016/j.ceramint.2015.12.130.
47. El-Shater RE, Assar ST, Keshta BE, Gemeay AH, El-Bahnasawy HH, Abdel-Khalek EK, Fakhry F. Synthesis and study on structural, magnetic, dielectric properties and impedance spectroscopy of nanosized Mn-doped γ-Fe2O3 for multifunctional applications. J Solgel Sci Technol. 2024;116(1):319–50. https://doi.org/10.1007/s10971-024-06579-3.
48. Rana AK, Kumar Y, Rajput P, Jha SN, Bhattacharyya D, Shirage PM. Search for origin of room temperature ferromagnetism properties in Ni-Doped ZNO nanostructure. ACS Appl Mater Interfaces. 2017;9(8):7691–700. https://doi.org/10.1021/acsami.6b12616.
49. Guglieri C, Céspedes E, Espinosa A, Laguna-Marco MÁ, Carmona N, Takeda Y, Okane T, Nakamura T, García-Hernández M, García MÁ, Chaboy J. Evidence of oxygen ferromagnetism in ZNO based materials. Adv Funct Mater. 2013;24(14):2094–100. https://doi.org/10.1002/adfm.201303087.
50. Espinosa A, Sánchez N, Sánchez-Marcos J, De Andrés A, Muñoz MC. Origin of the Magnetism in Undoped and Mn-Doped SnO2 Thin Films: Sn vs Oxygen Vacancies. J Phys Chem C. 2011;115(49):24054–60. https://doi.org/10.1021/jp205727b.

Figures

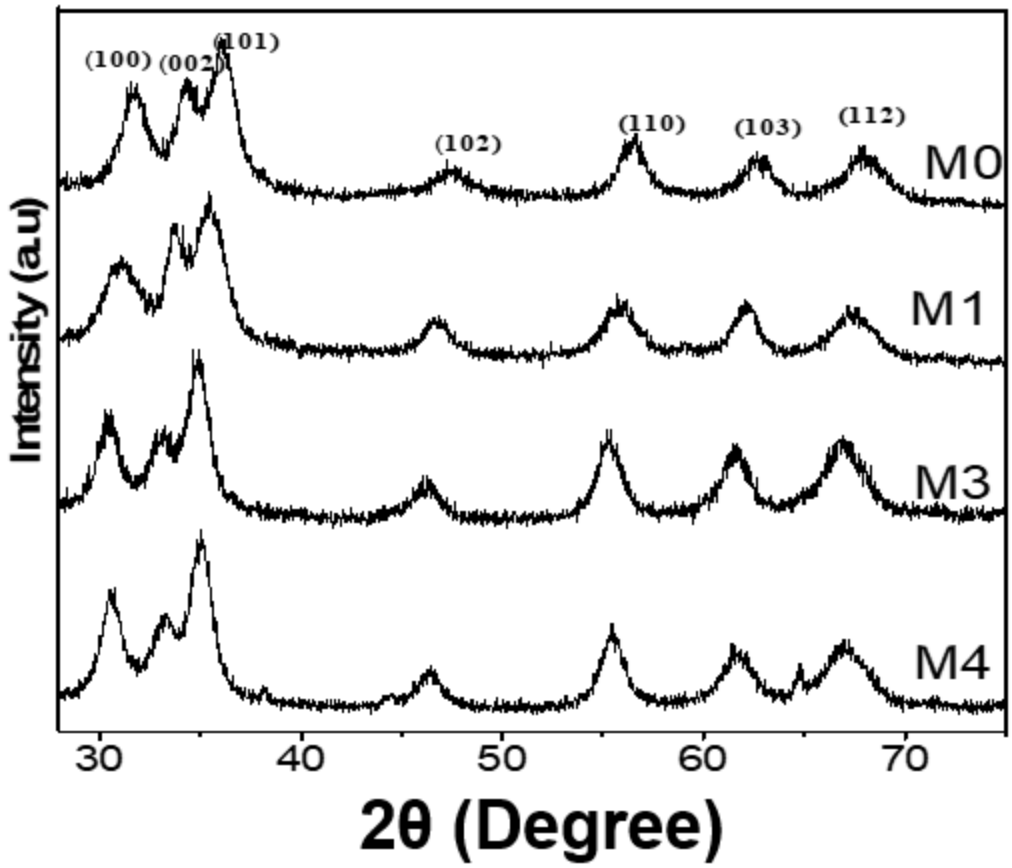


Figure 1

XRD patterns of pure ZnO and Mn doped ZnO nanoparticles.

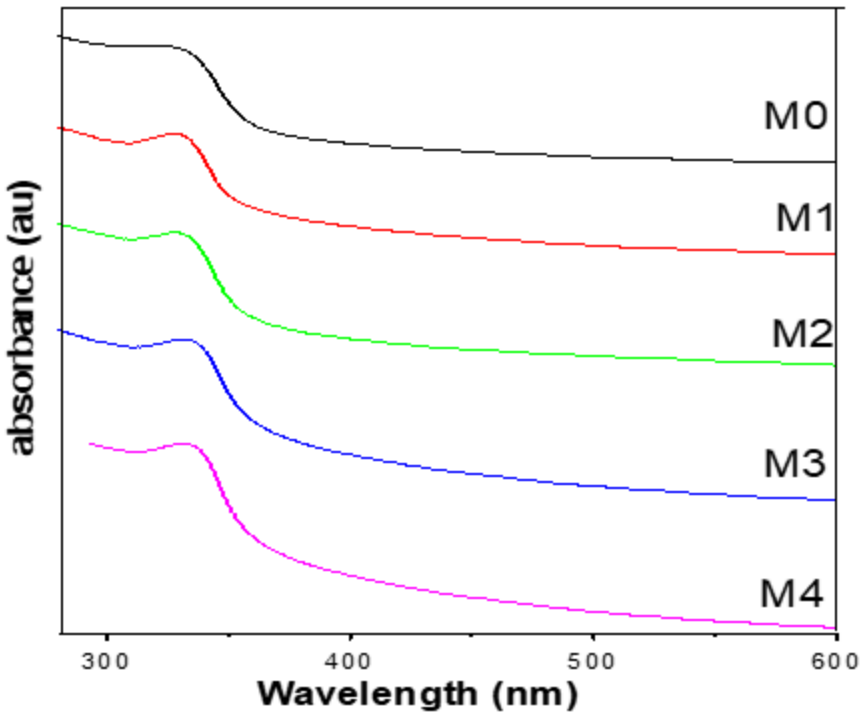


Figure 2

Optical absorption spectra of as synthesized undoped (M0) and doped ZnO nanoparticles(M1-M4).

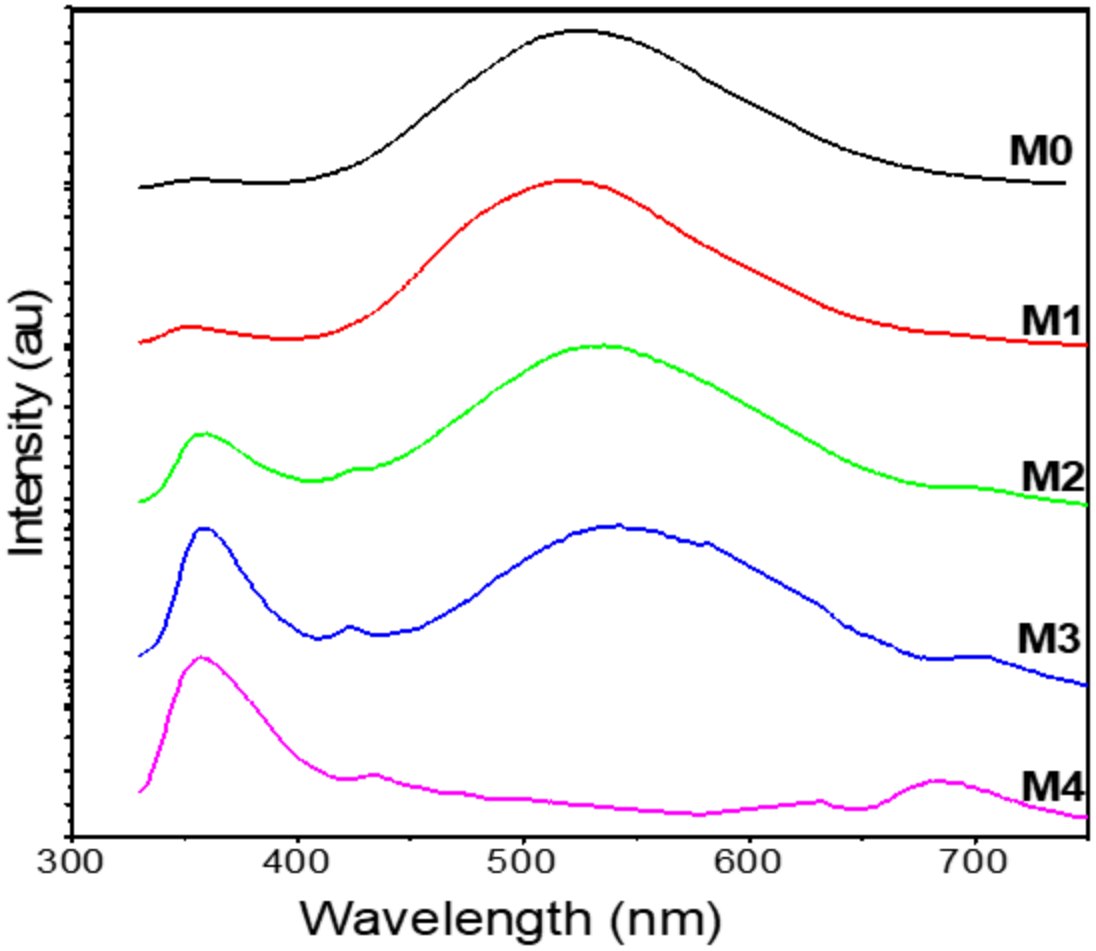


Figure 3

The room temperature photoluminescence spectra of undoped (M0) and Mn doped ZnO nanoparticles (M1 to M4).

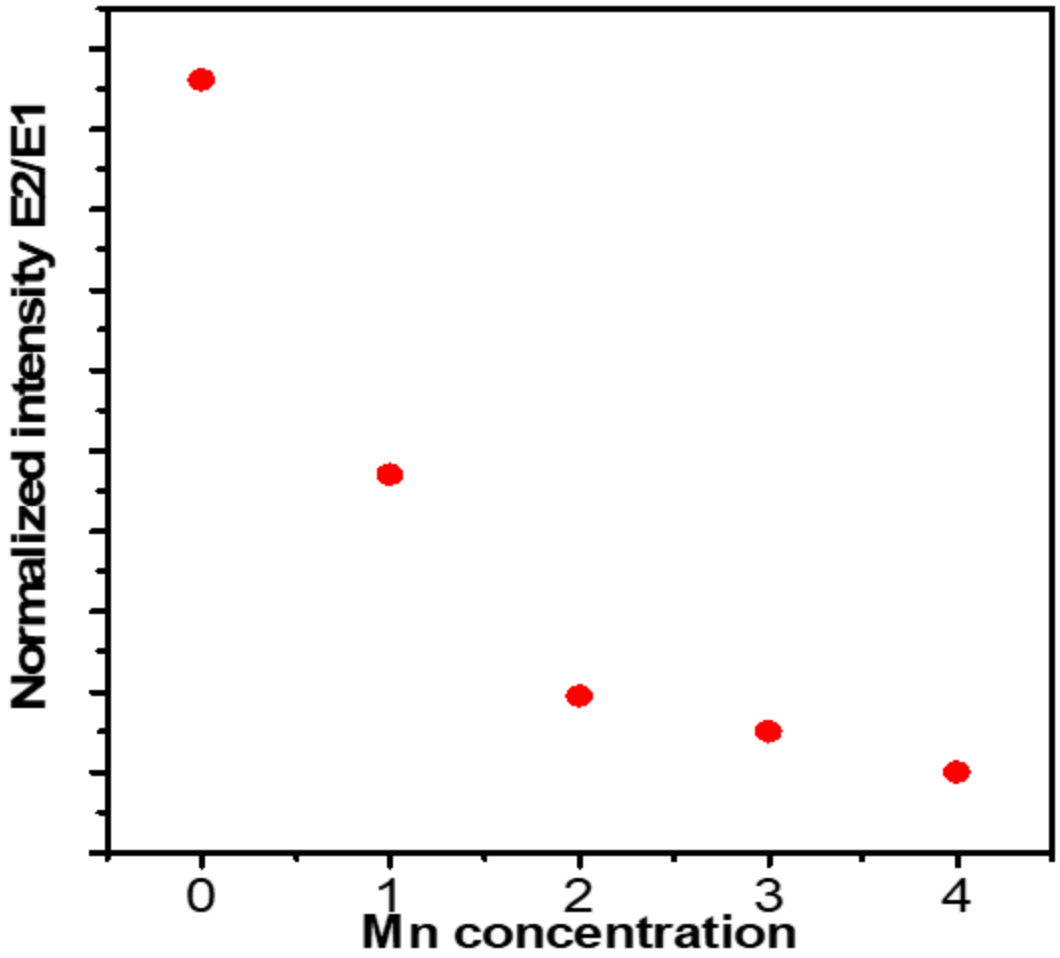


Figure 4

The normalized emission peak intensity (E1/E2) v/s Dopant concentration.

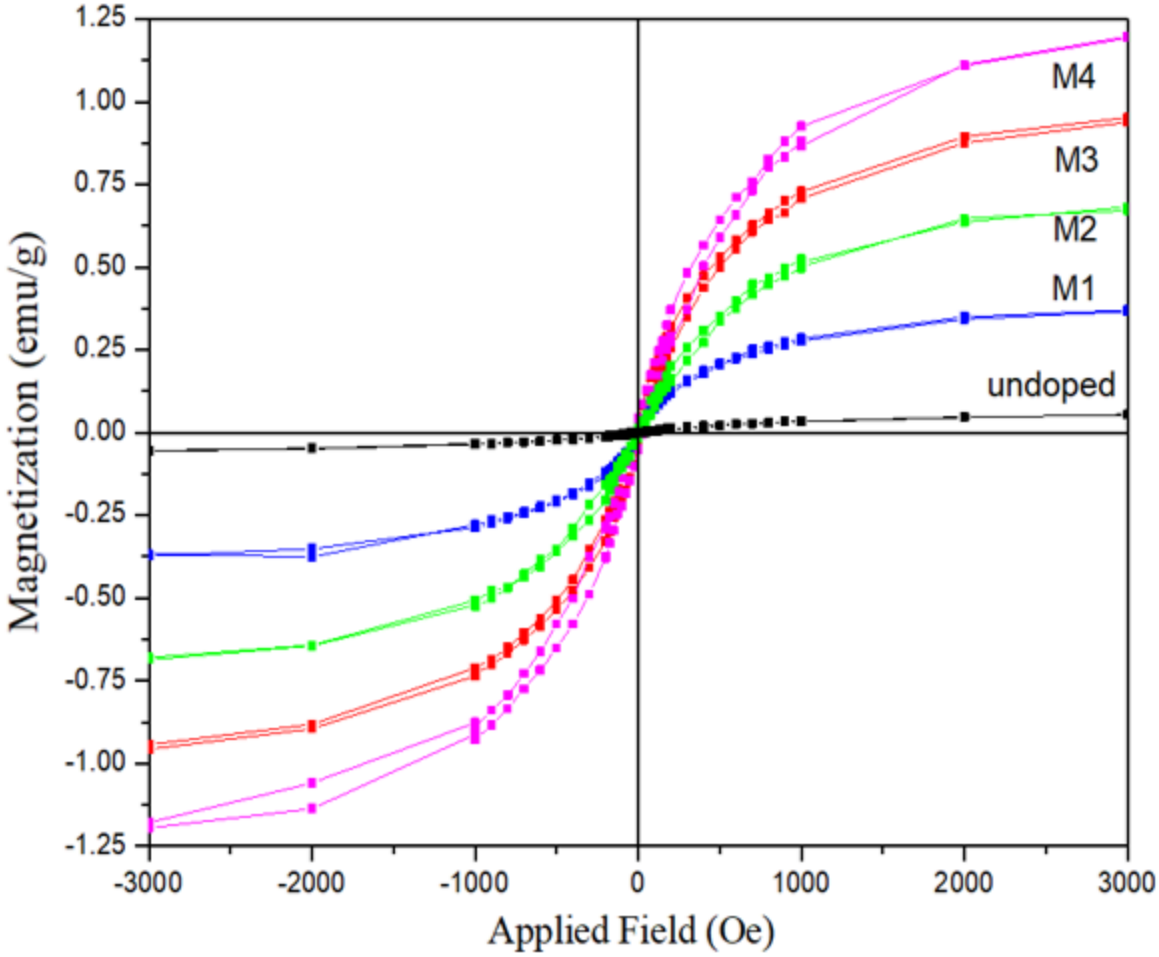


Figure 5

M-H loop generated by SQUID-VSM magnetometer forun-doped (M0) and Mn doped samples (M1toM4).

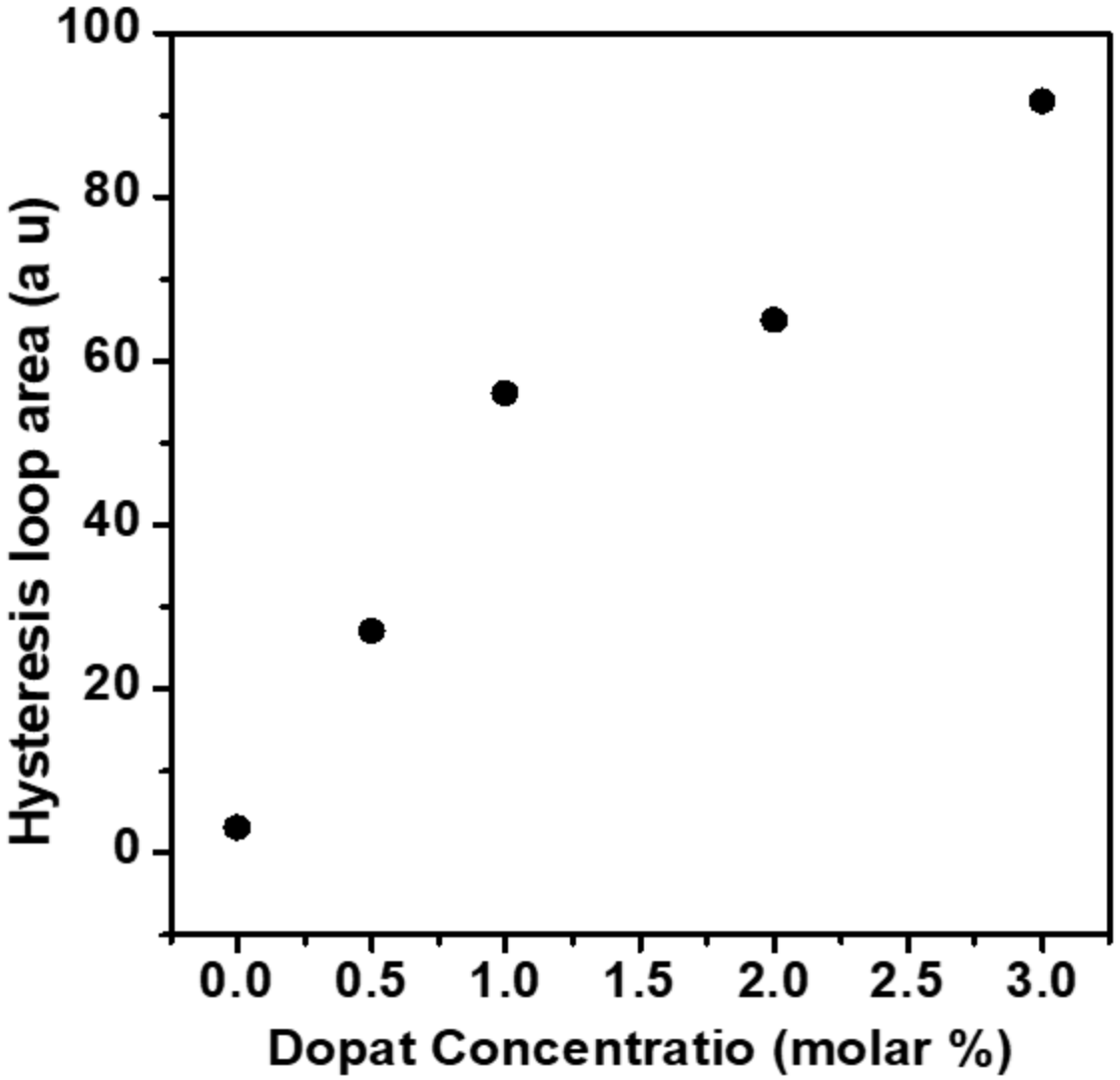


Figure 6

The plot of loop area calculated from the hysteresisloop for samples M0, M1, M2, M3 and M4 as function of dopant concentration.